ARTICLES

Chemical Dynamics of the OH and OD Radical Reactions with H_2S, CH_3SCH_3, and CH_3SH Studied by Infrared Chemiluminescence

N. I. Butkovskaya*

Institute of Chemical Physics, Russian Academy of Sciences, 117334 Moscow, Russian Federation

D. W. Setser

Department of Chemistry, Kansas State University, Manhattan, Kansas 66506

Received: November 19, 1997; In Final Form: May 27, 1998

The infrared chemiluminescence of H_2O and HOD molecules formed from the room-temperature reactions of OH and OD radicals with H_2S, CH_3SCH_3, and CH_3SH was recorded by viewing a fast-flow reactor with a Fourier transform spectrometer. Nascent vibrational distributions of the H_2O and HDO product molecules were obtained by computer simulation of the infrared spectra. According to our assignments for the $v_3 = 0$ populations, the vibrational distributions of HDO from the H_2S and CH_3SCH_3 reactions were inverted in the O−H stretching mode with a maximum in $v_3 = 2$ and $v_3 = 1$, respectively, and the fraction of the available energy released as vibrational energy is $\langle f_v \rangle \approx 0.6$ with ∼25−30% of the vibrational energy in the bending coordinate. The reaction with CH_3SH gives a HOD vibrational distribution that declines with increased v_3; $\langle f_v \rangle$ is only ≈0.4, but 40% of the vibrational energy is in the bending mode. For each reaction, the vibrational distributions for H_2O closely resemble those for HOD, after allowance is made for the collision-induced equilibration between the ν_1 and ν_3 modes of H_2O and the ν_1 and $2\nu_2$ modes of HOD. The reduced vibrational energy disposal to H_2O and HOD from CH_3SH is taken as evidence for a mechanism that differs from the direct abstraction process for the H_2S and CH_3SCH_3 reactions. These results are analyzed using information theory, and they also are compared with the data from similar reactions of hydroxyl radicals and F atoms. Secondary reactions of the sulfur-containing primary radicals (SH, CH_3S, and CH_3SCH_2) with NO_2 and NO are discussed.

1. Introduction

In recent work we have developed an infrared chemiluminescence method to determine the vibrational distributions of water molecules and deuterioanalogues produced in hydrogen abstraction reactions by hydroxyl radicals. The distributions are assigned by computer simulation of the spectra to obtain nascent vibrational distributions. The studies of the reactions with hydrogen halides (HBr,[1] HI[2] and HCl[3]), hydrocarbons (*n*-C_4H_{10}, neo-C_5H_{12}, and c−C_6H_{12})[3], GeH_4,[2] and NH_3,[3] revealed interesting features about the energy partitioning to the stretching and bending modes of H_2O and HOD. From these energy distributions, conclusions were made about the reaction mechanisms and dynamics. For example, the vibrational distributions of H_2O and HOD from the reactions of OH and OD with HBr and HI indicated a mechanism of direct abstraction for HBr and addition−elimination for HI. Since hydroxyl attack is one of the basic reactions in combustion and atmospheric chemistry and since understanding these complex processes is critically dependent on establishing the detailed mechanisms, our studies have been extended to aldehydes[4] and sulfur-containing molecules. The results from hydrogen sulfide, dimethyl sulfide (DMS), and methanethiol are presented in this paper.

Reactions of hydroxyl radicals with H_2S, DMS, and CH_3SH are the initial steps in the oxidation of these substances in thetroposphere: [5−23]

$$OH + H_2S \rightarrow H_2O + SH \quad (1)$$

$$OH + CH_3SCH_3 \rightarrow \text{products} \quad (2)$$

$$OH + CH_3SH \rightarrow \text{products} \quad (3)$$

The overall rate coefficients for reactions 1−3 have been extensively measured, and the recommended values are given in Table 1, along with the reaction enthalpies and available energies.

The agreement among the experimental values for k_1 is quite good, but the activation energy values range from 0.0 to 0.9 kcal mol^{-1}.[5,18−23] Although the products of reaction 1 are thought to be SH and H_2O,[5,18−22] no direct experimental proof has been reported. The discharge-flow measurements of the reaction rate constant, k_1, gave a curved Arrhenius plot, and

S1089-5639(98)00256-4 CCC: $15.00
Published on Web 07/17/1998

TABLE 1: Kinetic[a] and Thermodynamic[b] Data for the Reactions with H_2S, $(CH_3)_2S$, and CH_3SH

reaction	k(298 K)	E_a	D_0(R−H)	$-\Delta H^\circ_0$	$\langle E_{av}\rangle$[c]
$OH + H_2S \rightarrow H_2O + SH$	4.8 ± 0.7	0.16	89.9 ± 0.1[d,e]	28.2	30.8 ± 0.9
		0.82 ± 0.06[f]		28.9[g]	32.1[h]
$OH + DMS \rightarrow H_2O + CH_3SCH_2$	4.4 ± 0.4	0.47 ± 0.1	92.0 ± 1.4[i]	24.6[j]	27.5 ± 1.5
$OH + CH_3SH \rightarrow H_2O + CH_3S$	33 ± 4[k]	-0.7 ± 0.2[k]	86.1 ± 0.5[d]	32.0	34.4 ± 0.7
$\rightarrow H_2O + CH_2SH$			92.4 ± 2.0[d]	25.7	28.6 ± 2.0

[a] Recommended rate constants (in 10^{-12} cm^3 molecule^{-1} s^{-1}) and activation energies (in kcal mol^{-1}) were taken from ref 24. [b] Reaction enthalpies were calculated using $D_0(HO-H) = 118.08 \pm 0.03$ given in ref 25; all energy quantities are in kcal mol^{-1}. [c] Available energies were calculated according to expression $\langle E_{av}\rangle = -\Delta H^\circ_0 + E_a + 4RT$; the uncertainty in $\langle E_{av}\rangle$ for H_2S is a consequence of the uncertainty in E_a (see text). [d] Reference 25; [e] Reference 26. [f] Reference 23. [g] Reference 22. [h] Upper limit. [i] Reference 27. [j] Reference 13. [k] Overall value.

the suggestion has been made that OH reacts partly via addition to the S atom with subsequent rearrangement or elimination of a fragment. However, no adduct has been observed, and the rate constant shows no pressure dependence over the 0.8−3.5 Torr range.[20] The most recent ab initio study[22] for the H_2S reaction concluded in favor of only a direct abstraction pathway with an activation energy of 0.6 kcal mol^{-1}.

The possible channels of reaction 2 have been thoroughly reviewed.[5−11]

$$OH + CH_3SCH_3 \rightarrow H_2O + CH_3SCH_2 \quad (2a)$$

$$\rightarrow CH_3 + CH_3SOH \quad (2b)$$

$$\rightarrow CH_3S + CH_3OH \quad (2c)$$

$$\leftrightarrow CH_3S(OH)CH_3 \quad (2d)$$

In the absence of O_2 and at 298 K, the reaction proceeds mainly by hydrogen abstraction, channel 2a, while channels 2b and 2c are relatively unimportant.[5−4] In the atmosphere, reaction 2 proceeds either by hydrogen abstraction or by addition; these channels being completely separate processes.[9,11] The branching ratios for reaction 2 were studied with isotope labeling using OD and $(CD_3)_2S$.[9−11] The OD studies gave an HDO product yield of 0.84 ± 0.15[9a] with an upper limit to the CH_3 yield of 0.07, [10] showing that hydrogen transfer was the dominant channel. The adduct was directly observed in a pulsed laser photolysis/pulsed laser-induced fluorescence study,[11] and the estimated binding energy was ~11 kcal mol^{-1}. It was proposed that the thermalized $(CH_3)_2SOH$ adduct can dissociate back to reactants or react with oxygen;[9b,11] this view supersedes the suggestion that the adduct dissociates to other products.[12] The ratio of DMS to adduct is usually high enough that secondary reactions of OH with the adduct are not important. For the conditions of our experiments, only (2a) will be important.

The 7−8-fold larger rate constant for (3) vs (1) or (2) suggests a somewhat different mechanism. Although the HS−H bond is 2−3 kcal mol^{-1} weaker than the CH_3SCH_2−H bond,[25] the rate constants of reactions 1 and 2 per H atom, $k_1 = 2.4 \times 10^{-12}$ and $k_2 = 0.73 \times 10^{-12}$ cm^3 molecule^{-1} s^{-1}, differ only by a factor of 3, and in principle, reaction 3 can proceed by abstraction at both ends of the molecule. The addition pathway also has been discussed. Reaction 3 has been examined[14−16] under atmospheric conditions

$$OH + CH_3SH \rightarrow H_2O + CH_3S \quad (3a)$$

$$\rightarrow H_2O + CH_2SH \quad (3b)$$

$$\rightarrow CH_3S(OH)H \quad (3c)$$

using N_2 and O_2 buffer gases; the rate constant was the same as using Ar as a buffer gas, and the rate constant does not change with pressure. Tyndall and Ravishankara[6] showed that the CH_3S yield from reaction 3 was unity, but they could not exclude a process involving $CH_3S(OH)H$ that eliminates H_2O to give CH_3S.[6] Wine et al.[15,16] studied the reactions of CD_3SH and CH_3SD with OH. The kinetic isotope effects were very small for both molecules, and Wine et al.[15,16] suggested that the major pathway must be addition of OH to the sulfur atom of CH_3SH. Mechanistic interpretation of small kinetic isotope effects for reactions with no potential barriers is not straightforward, and conclusions based on the kinetic isotope effects regarding (3a) vs (3b) have not been reached. The recent ab initio study[17] of the OH + CH_3SH reaction suggested that formation of the adduct is slightly (1.4 kcal mol^{-1}) endothermic and that the abstraction reaction has no activation barrier. The authors concluded that the reaction proceeds via abstraction of the sulfur-bonded hydrogen.

Direct observation of the products and knowledge of the vibrational distributions of H_2O and HOD from reactions 1−3 would increase our understanding. Also, such data add to our basic knowledge about the **H−L−H** class of molecular dynamical systems yielding triatomic products.[1−4] The available reaction energy is sufficient to excite up to three stretching quanta in the water molecule produced in reactions 1 and 3 and two stretching quanta in reaction 2. The chemiluminescent infrared spectra from reactions 1−3 and the analogous reactions

$$OD + H_2S \rightarrow HDO + SH \quad (1D)$$

$$OD + CH_3SCH_3 \rightarrow HDO + CH_2SCH_3 \quad (2D)$$

$$OD + CH_3SH \rightarrow \text{products} \quad (3D)$$

with OD were recorded using a fast-flow reactor with a Fourier transform spectrometer in the KSU laboratory. Hydroxyl radicals were obtained via the fast H (D) + $NO_2 \rightarrow$ OH (OD) + NO reaction. The H_2O and HOD spectra in the 3200−3900 and 2400−3900 cm^{-1} ranges, respectively, will be presented. The H_2O and HOD vibrational distributions were determined from these spectra, and the information−theoretic analysis was used to discuss these distributions. The discussion includes a comparison of the results obtained from reactions 1−3 with results from the OH and OD reactions with hydrocarbons and with the analogous reactions of F atoms. The secondary reactions of the primary radicals HS, CH_3S, and CH_3SCH_2 with NO_2, OH, and NO could be observed in our apparatus. Although this was not the main goal of the present work, some products from the secondary reactions have been detected by infrared chemiluminescence. Since these reactions are important

for schemes of atmospheric oxidation of sulfur-containing compounds, they are considered as well.

2. Experimental Section

2.1. Experimental Apparatus and Techniques. The experimental setup and procedures have been described in preceding papers.[1−3] The infrared chemiluminescence spectra from vibrationally excited H_2O and HDO molecules were recorded by a Fourier transform infrared spectrometer (BIO-RAD), which viewed the fast-flow reactor through a NaCl window. Each spectrum consists of an average of 512 scans of the spectrometer with a spectral resolution of 1 cm^{-1}. The OH or OD radicals were produced via the reaction of H or D with NO_2 in the prereactor section of the flow reactor. The H or D atoms were generated by a microwave discharge of H_2 (D_2)/Ar mixtures. The reactants were introduced into the reactor through a ring injector located 20 cm downstream of the hydrogen and nitrogen dioxide inlets and 3.5 cm upstream of the observation window. For a total pressure of 0.5 Torr, the flow velocity was about 140 m s^{-1}, corresponding to a reaction time of $\Delta t \sim 0.2$ ms. The concentration of H or D atoms was in the range $(2-4) \times 10^{13}$ molecules cm^{-3}; the NO_2 concentration was maintained between 4×10^{13} and 10×10^{13} molecules cm^{-3}. Reactant concentrations (in molecules cm^{-3}) were $[H_2S] = (1-3) \times 10^{13}$, $[DMS] = (4-7) \times 10^{13}$, and $[CH_3SH] = (2-6) \times 10^{13}$. Secondary reactions in the systems (1)−(3) are considered below. No OH or NO emission was observed when running the H + NO_2 reaction in the absence of an added reagent.

Commercial tank grade Ar was passed through three molecular sieve traps cooled by acetone/dry ice mixture and liquid N_2. The sulfur compounds were purified by several freeze−thaw−pump cycles and stored as 20% mixture in 10 L glass reservoirs. Tank grade H_2 and D_2 were used without purification.

2.2. Data Treatment. We have shown[1−3] that the H_2O and HOD spectra are not affected by vibrational relaxation for experiments at <0.7 Torr and $\Delta t < 0.3$ ms. However, collision-induced equilibration between ν_1 and ν_3 modes of H_2O and similar equilibration between the ν_1 and $2\nu_2$ modes in HOD occurs even at 0.3 Torr, so only the distributions in the $\nu_{1,3} + \nu_2$ and $\nu_{1,2} + \nu_3$ reservoirs, respectively, can be assigned. The data were obtained for 0.5 Torr and $\Delta t < 0.25$ ms, so the previous discussion about the absence of vibrational relaxation is valid.[1−3] Except for the equilibration mentioned above, and a slight reservation[1] about the possible relaxation of $\upsilon_{1,2}$ levels of HOD above $\upsilon_2 = 4$, the spectra should yield nascent vibrational distributions.

Vibrational populations were obtained by computer simulation of the spectra, after correction for the variation of the detector's response function with wavelength. The simulation method is based on the calculation of H_2O and HOD fundamental emission bands from the known ν_1, $2\nu_2$, and ν_3 absorption bands,[28] assuming a cubic dependence of the emission intensity upon the transition frequency and Boltzmann rotational population. The details of the calculation were described earlier.[1,2] The HOD chemiluminescent spectra observed in 3200−3900 cm^{-1} range were modeled by superposition of emission bands corresponding to $\Delta\nu_1 = -1$ and $\Delta\nu_3 = -1$ transitions from $(\upsilon_{1,3},\upsilon_2)$ vibrational states with $\upsilon_{1,3} = \upsilon_1 + \upsilon_3 \leq 3$ and $\upsilon_2 \leq 5$. The HOD spectra consist of two parts: a 3200−3900 cm^{-1} range that can be simulated by fundamental and combination bands, corresponding to $\Delta\nu_3 = -1$ transitions from $\upsilon_3 \leq 3$, $\upsilon_{1,2} \leq 5$ levels, and a 2400−3000 cm^{-1} range composed of $\Delta\nu_1 = -1$ and $\Delta\nu_2 = -2$ transitions from a variety of levels including $\upsilon_3 = 0$. The notation $\upsilon_{1,2}$ is used to denote the group of the equilibrated levels, $(\upsilon_1, \upsilon_2, \upsilon_3)/(\upsilon_1 + i, \upsilon_2 - 2i, \upsilon_3)$, $i = 0, 1, ...$, and refers to the maximum υ_2 number ($i = 0$) in the group. The 2400−3000 cm^{-1} spectra permit an assignment of the population in the $\upsilon_3 = 0$ stretching state, except for the dark (000) and (010) states. In the present work, the populations in these states were taken as equal to the population in the (020)/(100) and (030)/(110) equilibrated pairs, respectively. The simulation was made using a least-squares procedure over the whole spectrum with normalization to the highest peak in the spectrum.

TABLE 2: Vibrational Distribution of H_2O from the Reactions of OH with Hydrogen Sulfide, Dimethyl Sulfide, and Methanethiol

	υ_2								
$\upsilon_{1,3}$[a]	0	1	2	3	4	≥5	$P_{1,3}$[b]	$P_{1,3}$[c]	$P_{1,3}°$
					H_2S				
0[d]	2.6	4.5	3.6	1.7	0.9	0.6	(13.8)	12.2	55.9
1	10.3	17.7	14.3	6.6	0.8		49.7	43.6	34.6
2	24.4	20.6	0.8				45.8	40.2	9.37
3	4.5						4.5	4.0	0.1
P_2[e]	36.7	37.6	16.4	7.3	1.5	0.5			
$P_2°$	44.8	26.6	14.9	7.9	3.8	2.1			
					CH_3SCH_3				
0[d]	11.4	14.9	7.3	3.5	1.7	0.6	(39.3)	28.2	63.2
1	20.4	26.7	13.1	6.3			66.5	47.7	32.2
2	21.5	12.0					33.5	24.0	4.6
P_2[e]	38.3	38.5	14.6	7.0	1.2	0.4			
$P_2°$	46.8	27.3	14.7	7.1	3.1	1.1			
					CH_3SH				
0[d]	20.6	26.8	15.3	9.2	4.5	2.9	(79.4)	44.6	52.6
1	19.1	24.8	14.2	8.5	2.4		69.1	38.8	35.2
2	15.4	11.4	0.8				27.6	15.7	11.5
3	3.3						3.3	1.8	0.7
P_2[e]	32.6	35.1	16.9	9.9	3.8	1.6			
$P_2°$	41.1	26.2	15.7	8.9	4.7	3.1			

[a] $\upsilon_{1,3} = \upsilon_1 + \upsilon_3$. [b] $P_{1,3}(0)$ is neglected. [c] $P_{1,3}(0)$ as estimated from linear surprisal plots for model I for prior calculation; the $P_{1,3}(1)/P_{1,3}(2)$ ratios are thought to have an uncertainty of 9% (see text for discussion of the assignment of uncertainties). [d] Bending distribution in $\upsilon_{1,3} = 0$ is assumed to be similar to the one in $\upsilon_{1,3} = 1$ and extended to $\upsilon_2 = 6$ according to a geometric progression. [e] Normalized distribution.

The reader must be aware of the differences between a $P_{1,3}$ distribution of H_2O and a P_3 distribution of HOD and between a P_2 distribution for H_2O and a $P_{1,2}$ distribution of HOD. The $P_3(\upsilon_3)$ distribution is a sum of populations over all υ_1 and υ_2 numbers for a given υ_3 value, while $P_{1,3}$ is a sum over υ_2 for a given $\upsilon_1 + \upsilon_3$. For example, considering a hypothetical stretching distribution $\{P(\upsilon_1 = 0, \upsilon_3 = 0) = a, P(\upsilon_1 = 1, \upsilon_3 = 0) = b, P(\upsilon_1 = 0, \upsilon_3 = 1) = c, P(\upsilon_1 = 1, \upsilon_3 = 1) = d\}$, we have $P_3(0{:}1{:}2) = (a + b){:}(c + d){:}\ 0$ and $P_{1,3}(0{:}1{:}2) = a{:}(b + c){:}d$. The difference between P_2 and $P_{1,2}$ is more complicated because of the multiplicity of energies of ν_1 and ν_2 quanta. The former is a simple summation over υ_1 and υ_3 quantum numbers for all the states with a given υ_2 number. Thus, if we suppose that in the above example every stretching state has some bending distribution up to $\upsilon_2 = 2$, then $P_2(0{:}1{:}2) = (a_0 + b_0 + c_0 + d_0){:}(a_1 + b_1 + c_1 + d_1){:}(a_2 + b_2 + c_2 + d_2)$, where a subscript denotes a bending quantum number. In this case, $P_{1,2}$-$(0{:}1{:}2{:}3{:}4) = (a_0 + c_0){:}(a_1 + c_1){:}(a_2 + b_0 + c_2 + d_0){:}(b_1 + d_1){:}(b_2 + d_2)$. Quantitative differences in these distributions may be seen from comparison of the calculated statistical distributions $P°_{1,3}$ vs $P°_3$ and $P°_2$ vs $P°_{1,2}$ for the (1,1D), (2,-2D), and (3,3D) reactions presented in Tables 2 and 3.

TABLE 3: Vibrational Distribution of HDO from the Reactions of OD with Hydrogen Sulfide, Dimethyl Sulfide, and Methanethiol

	$v_{1,2}$[a]										
v_3	0	1	2	3	4	5	6	7	P_3[b]	P_3[c]	$P_3°$
						H_2S					
0	6.3[d]	1.1[d]	6.3	1.1	1.7	1.1	1.6	0.8	20 ± 7	14.9 ± 3.3	77.0
1	9.1	4.2	10.7	1.5	2.4	1.9			29.8	31.7	20.0
2	24.2	9.3	9.2	4.6					47.2	50.2	2.91
3	3.0								3.0	3.1 ± 0.4	0.053
$P_{1,2}$	42.6	14.6	26.2	7.2	4.1	3.0	1.6	0.8			
$P_{1,2}°$	24.8	17.1	22.4	13.7	11.6	5.9	3.4	0.9			
						CH_3SCH_3					
0	6.2[d]	1.9[d]	6.2	1.9	3.2	2.2	2.5	1.0	25 ± 9	33.1 ± 3.8	81.8
1	23.7	3.4	10.7	7.7	2.6				48.0	42.8	16.8
2	20.2	3.5	3.3						27.0	24.0	1.40
$P_{1,2}$	50.1	8.8	20.2	9.6	5.8	2.2	2.5	1.0			
$P_{1,2}°$	27.4	18.1	23.3	13.6	10.7	4.8	2.0	0.1			
						CH_3SH					
0	13.2[d]	10.8[d]	13.2	10.8	5.4	5.0	2.6	2.5	63.4 ± 8	60.2 ± 3.7	74.8
1	10.5	3.2	4.8	2.0	0.7	0.4			21.5	23.4	21.3
2	9.0	3.6	0.8	0.7					14.1	15.3	3.78
3	1.0								1.0	1.1 ± 0.4	0.18
$P_{1,2}$	33.7	17.6	18.8	13.5	6.1	5.4	2.6	2.5			
$P_{1,2}°$	21.4	15.4	21.3	13.8	13.0	7.3	5.0	2.1			

[a] See section 2.2 for the definition of $v_{1,2}$. [b] $P_3(0)$ from simulation; the $P_3(1)/P_3(2)$ ratios are thought to have an uncertainty of 6% (see text for discussion of uncertainties). [c] $P_3(0)$ from linear surprisal plots for model I prior calculation. [d] Populations in the dark (000) and (010) states were assumed to be equal to populations in the (020)/(100) and (030)/(110) states, respectively. Comparison with the P_2 distribution of H_2O suggest that this is an underestimate of the $P_{1,2}(1)$ population for reactions 1 and 2.

The $H_2O(v_{1,3}=0)$ populations were estimated using the information−theoretic analysis developed by Bernstein and Levine[29] with extension to include reactions that gave triatomic H_2O, HOD, and D_2O products.[1] Linear vibrational surprisal plots have been found for reactions of OH and OD radicals with HBr, HI, and GeH_4 with excitation of three or four stretching quanta.[1,2] Since only two experimental points exist on the surprisal plot for the DMS reaction, the linearity was taken for granted to estimate $P_{1,3}(0)$. However, the validity of the linear extrapolation was confirmed by the HOD data, which provide experimental values for the $v_3 = 0$ population. The prior distributions, $P°_{1,2}$ and $P°_3$, which are given in Tables 2 and 3, were calculated using a model that treated the radical product as an atom (model I). We also examined surprisal plots using priors that took into account the rotational degrees of freedom of the radical fragment (model II).

2.3. Reliability of the Simulations. We shall analyze three sources of uncertainty in the vibrational populations obtained from the simulation. The first one is the uncertainty in the least-squares method of fitting, which can be evaluated using a least-squares formalism that has been described.[1] In the simulation, every emission band is considered as a vector with $N = 1452$ elements corresponding to the number of measurements in one spectrum. For measurements of equal accuracy, the least-squares method requires a minimization of the value of the estimator $Q = \sum(s_i - \sum P_j b_{ij})^2$, where s_i is the ith measurement in the experimental spectrum, b_{ij} is the ith element of the jth basic band, and P_j are the populations of the corresponding vibrational states. The inner summation is made over the basic vectors, and the outer one is a summation over all elements of the spectrum. The standard deviation of the populations is estimated by $\sigma(P_i) = [(G)^{-1}_{ii}Q/N]^{1/2}$, where $(G)^{-1}_{ii}$ is the diagonal element of the reciprocal Gram's matrix of the basic vectors $b_i = (b_{1i}, b_{2i}, ..., b_{Ni})$, i.e., $C_{kl} = b_k T b_l$. The values of $(G)^{-1}_{ii}$ obtained in fitting the H_2O spectra from the OH + HBr reaction[1] varied from 2.7×10^6 to 4.4×10^6. In the present study, the largest least-squares estimator, $Q = 1.7 \times 10^6$, was obtained for the H_2O spectrum from reaction 1, because it had the most noise of the six spectra. This Q gives a standard deviation for the populations of $\sigma(P_i) \approx 0.07$, which can be considered as the upper limit for the $\sigma(P_i)$ of $v_{1,3} = 1$ and 2 in the H_2O populations in reactions 1−3. The uncertainties for $v_{1,3} = 0$ and 3 are discussed below. The $\sigma(P_i)$ values for HOD populations in $v_3 = 1$ and 2 are about 0.04, because the HOD fitting is more accurate, $Q = 1.0 \times 10^6$, 7.5×10^5, and 5.8×10^5 for reactions 1D, 2D, and 3D, respectively. Thus, we can conclude that $P(1)/P(2)$ ratios are determined with an accuracy better than 9% and 6% for the H_2O and HDO distributions, respectively. These values correspond only to the uncertainty in the simulation and do not include experimental errors associated with acquiring the spectra or errors in the basic vectors.

Another source of error arises from the uncertainty in the baselines of the FTIR spectra, which are obtained as the difference between the reaction and background spectra calculated, respectively, from the interferograms measured with and without the reagent. The position of the baseline is especially important in fitting the highest v_3 bands, which have contributions of only a few percent, and in the fitting of the $\Delta v_1 = -1/\Delta v_2 = -2$ part of the HOD spectra with an intrinsically low intensity. To evaluate the magnitude of these uncertainties, we determined a standard deviation σ_0 of the linear fitting of the baseline and then performed the simulation procedure for the $\pm\sigma_0$ limit cases. Such tests gave error limits of 4.5 ± 0.7% and 3.3 ± 0.4% for $P_{1,3}(3)$ for reactions 1 and 3 and 3.1 ± 0.4% and 1.0 ± 0.4% for $P_3(3)$ for reactions 1D and 3D. For the HOD $P_3(0)$ populations, the error limits due to baseline are ±4%, ±4%, and ±1.5% for reactions 1D, 2D, and 3D, respectively. A somewhat larger error is introduced by the need to estimate the populations of the dark states; these uncertainties were chosen as half of the population in (020)/(100) states: 2.3, 4.1 and 6.6% for reactions 1D, 2D, and 3D, respectively. The total uncertainty for the measured $P_3(0)$ are indicated in (column P_3[b]) of Table 3. The error limits for $P_{1,3}(0)$ and $P_3(0)$

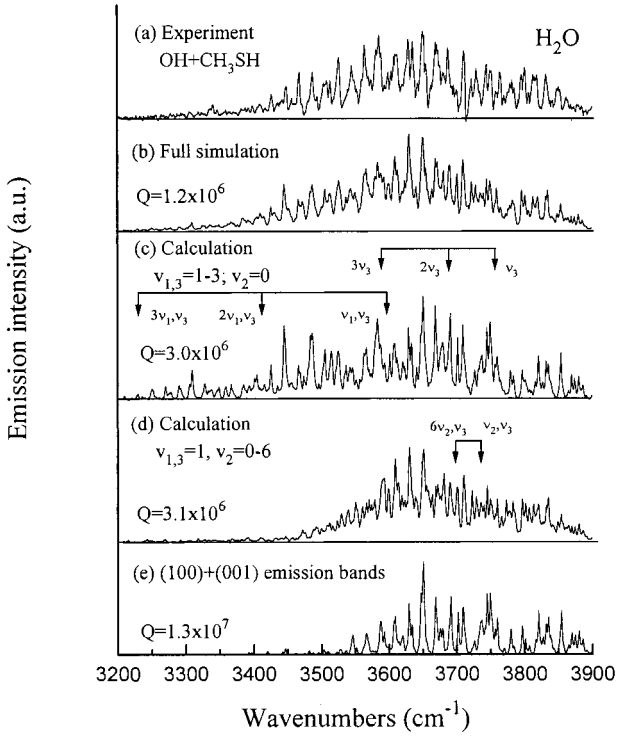

Figure 1. Simulation of the H_2O chemiluminescent spectrum from the OH + CH_3SH reaction: (a) experimental spectrum; (b) the best fit for a full set of possible vibrational states; (c) the best fit for stretching excitation; (d) the best fit for transitions from $\upsilon_{1,3} = 1$ with added bending excitation; (e) the fundamental emission bands (001) and (100). All fitting are with normalization to the total intensity. *Q* is the least-squares estimator (see text).

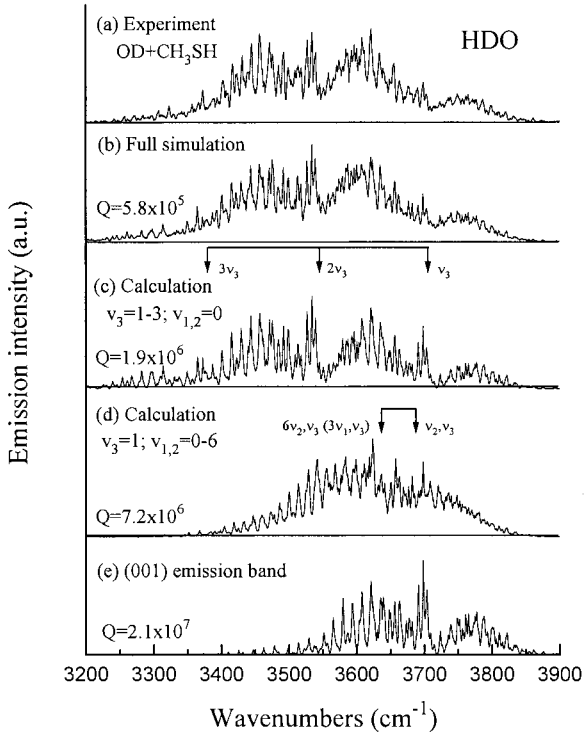

Figure 2. Simulation of the HOD chemiluminescent spectrum from the OD + CH_3SH reaction: (a) experimental spectrum; (b) the best fit for a full set of possible vibrational states; (c) the best fit for stretching excitation; (d) the best fit for transitions from $\upsilon_3 = 1$ with added bending excitation; (e) the fundamental (001) emission bands. All fitting are with normalization to the total intensity. *Q* is the least-squares estimator (see text).

estimations obtained from linear surprisal plots are presented in Tables 2 and 3 in columns $P_{1,3}{}^c$ and $P_3{}^c$. They correspond to the standard deviations of the intercepts as given by linear regression fitting and reported in section 3.

The last question is how unique are the obtained populations.[1−3] Some models for the H_2O and HDO spectra from reactions with CH_3SH are presented in Figures 1 and 2 in order to elucidate the respective roles of stretching and bending excitations in fitting the observed emission. The fundamental bands with a 300 K Boltzmann rotational distribution are presented at the bottom of Figures 1 and 2. They obviously do not reproduce the experimental spectra shown at the top; the least-squares estimators, $Q = \sum(s_i - b_i)^2$, where s_i is the *i*th measurement of the spectrum and b_i is the *i*th element of the (001) band, are of the order of 10^7. Addition of combination and hot bands to the computed spectrum is necessary. The bands with $\upsilon_3 = 1$ and nonzero υ_2 and υ_1 are red-shifted, relative to the fundamental (001) band, by $|x_{23}|$, $|x_{13}|$, and $2|x_{33}|$, respectively. The substantial differences in the H_2O anharmonicity coefficients, $x_{23} = -20.3$, $x_{13} = -165.8$, and $x_{33} = -47.6$ cm^{-1}, enable us to distinguish bending and stretching excitations. The band centers for $(0\upsilon_2 1)$ bands with $\upsilon_2 = 0-4$ are precisely known, as well as the correct positions for all rotational transitions. The actual shift due to the bending excitation is 19.4, 36.1, 48.9, and 56.4 cm^{-1} for $\upsilon_2 = 1$, 2, 3, and 4, respectively. The spectral range of $(0\upsilon_2 1)$ bands with $\upsilon_2 = 0-4$ does not overlap with the (002) band with stretching excitation, and the fitting error would be only due to the uncertainties in transition intensities, which is not expected to be important. The positions for the $\upsilon_2 = 5$ and 6 bands are not known so precisely; the uncertainty is about 10 cm^{-1}, and only the total population of $\upsilon_2 \geq 5$ levels can be stated with confidence. The positions of the band centers from (011) to (061) are indicated by arrows in Figure 1d. The estimator $Q = 3.1 \times 10^6$ was obtained for the calculated spectrum shown in Figure 1d, which contains only $(0\upsilon_2 1) + (1\upsilon_2 0)$ bands with a distribution of $P_2(0-5) = 22$, 24, 19, 15, 13, and 9. It is clear that bending excitation alone cannot account for the emission in the 3200−3600 cm^{-1} range. Next a calculation corresponding to a superposition of bands with stretching excitation only, (001) + (100), (002) + (101) + (200), and (003) + (102) + (201) + (300), is shown in Figure 1c. The upper set of arrows shows the position of the centers of (001), (002), and (003) bands; the lower set indicates the position of the (101), (201), and (301) band centers. These bands cover the required spectral range, but the calculated spectrum does not reproduce the shape of the experimental spectrum; the best fitting is $P_3(1-3) = 51$, 31, and 18, but the $Q = 3.0 \times 10^6$ is similar to that of the previous bending model. Only combination of both bending and stretching excitation as in Figure 1b allows satisfactory agreement with the experimental spectrum. Most of the observed peaks are reproduced with the populations given in Table 3, and the *Q* value is 1.0×10^6. The band positions of certain stretch and bend combination do have similar positions. For example, the shifts of the (051) and (002) bands are rather close, 60 and 66.8 cm^{-1}, but populations of these states can still be separated owing to the different positions of the emission from the coupled levels in the stretching reservoir. For example, the mixed levels (051)/(150) and (002)/(101)/(200) give different basic spectra, unlike the similar (051) and (002) bands. An additional check on the division between bending and stretching excitation is the comparison between H_2O and HOD distributions from the same reaction.[1−3]

Obtaining the υ_3 populations from the HOD spectra is more accurate because of the P, Q, R structure with the characteristic

Q-branch peaks (see Figure 2e with the fundamental band). As for H_2O, different υ_3 bands are widely separated by the anharmonic shift, $2|x_{33}| = 165.8$ cm^{-1} (see arrows in Figure 2c), while excitation of the coupled υ_1 and υ_2 levels gives a shift of only 13.1 and 20.1 cm^{-1}, respectively (see Figure 2d), and the total populations of the $\upsilon_3 = 1$ and $\upsilon_3 = 2$ states can be determined accurately. The least-squares estimators are $Q = 2.1 \times 10^7$ for the (001) fundamental band; $Q = 7.2 \times 10^6$ for a bending excitation within the $\upsilon_3 = 1$ state up to $\upsilon_2 = 6$ with $P_{1,2}(0-6) = 12$, 9, 0, 0, 4, 7, and 68; $Q = 1.9 \times 10^6$ for a ν_3 stretching excitation of $P_3(1-3) = 48$, 45, and 7; and $Q = 5.8 \times 10^5$ for the best simulated spectrum, which corresponds to the distribution in Table 3. The extremely nonphysical bending distribution associated with just $\upsilon_1 = 1$ excitation is the bending distribution that gave the smallest Q value.

3. Experimental Results

3.1. Reactions of OH and OD with H_2S. The H_2O and HOD spectra from reactions 1 and 1D are shown in Figures 3a and 4a, respectively. They were recorded at 0.5 Torr and the reactant concentrations indicated in the figure captions. The calculated spectra presented by the dotted curves are the best fit vibrational distributions given in Tables 2 and 3 for H_2O and HOD. The stretching distribution for nonzero levels of H_2O, $P_{1,3}(1{:}2{:}3) = 50{:}46{:}4$, has a slightly higher population for $\upsilon_{1,3} = 1$ than for $\upsilon_{1,3} = 2$, and a ~0.04 contribution from $\upsilon_{1,3} = 3$ was needed. The bending distribution of $\upsilon_{1,3} = 1$ has a slight inversion with a maximum population in $\upsilon_2 = 1$. The energies of the vibrational levels with $\upsilon_{1,3} = 3$ are 30.2 (300), 30.3 (201), 31.1 (102), and 31.5 kcal mol^{-1} (003), which are very close to the available reaction energy, $\langle E_{av}\rangle = 30.8$ kcal mol^{-1}, as calculated from the recommended $E_a = 0.16$ and $\Delta H°_0 = -28.2$ kcal mol^{-1}. Taking into account the uncertainties of the HS−H bond energy and activation energy of reaction 1, about 1.5 kcal mol^{-1} in total, the excitation of $\upsilon_{1,3} = 3$ is thermochemically possible. Due to the closeness of $\langle E_{av}\rangle$ to the energy needed for excitation of three stretching quanta, the $P_{1,3}(3)$ point could not be included in the surprisal analysis, because the prior distribution near the energy limit is extremely sensitive to $\langle E_{av}\rangle$. Solving the inverse problem, $\langle E_{av}\rangle = 32.1$ kcal mol^{-1} satisfies the linear surprisal plot that included all three points ($\upsilon_{1,3} =$ 1,2,3). From this value for the available energy, taking the upper limit for $\Delta H°_0 = -28.9$ kcal mol^{-1}, an activation energy of $E_a = 0.8$ kcal mol^{-1} can be deduced. This value substantially exceeds the recommended $E_a = 0.16$ kcal mol^{-1},[24] but it is consistent with $E_a = 0.79 \pm 0.38$ kcal mol^{-1} from the measurements of Lafage et al.[23a] or $E_a = 0.88$ kcal mol^{-1} given by Westenberg and de Haas.[23b] The most recent ab initio study[22] favored $E_a = 0.62$ kcal mol^{-1}. Our analysis of the energy disposal will be done using $\langle E_{av}\rangle = 32.1$ kcal mol^{-1}.

The H−OD distribution is clearly inverted, $P_3(0{:}1{:}2{:}3) = 20{:}30{:}47{:}3$, with a maximum on $\upsilon_3 = 2$. The energy of HOD-(003) is 30.4 kcal mol^{-1}, while the available energy, after correction for zero-point energy of reactants and products, is ≈32.4 kcal mol^{-1}. The emission intensity from $\upsilon_3 = 0$ (the 2500−2900 cm^{-1} part of the spectrum) was rather low, and the value given by least-squares analysis must be considered as approximate. However, the estimate of $P_3(0)$ made using a surprisal analysis gave a similar result. The $P_{1,2}(\upsilon_{1,2})$ distribution is similar to $P_2(\upsilon_2)$ from H_2O, which is indicative that the "old" OD bond did not receive much energy. The $P_{1,2}$ (1) population of HOD seems anomalously low when compared to the $P_2(1)$ population of H_2O; this probably is an artifact from the background subtraction procedure and the way that we estimated the population of the dark states.

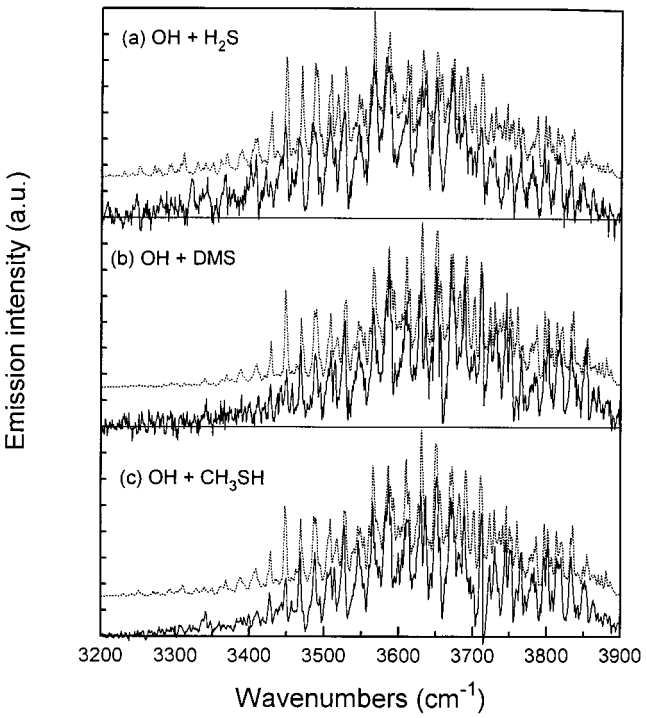

Figure 3. Infrared chemiluminescent spectra produced by the reactions of OH at 0.5 Torr ($\Delta t = 0.25$ ms): (a) with H_2S, $[NO_2] = 4 \times 10^{13}$, $[OH] = 2.2 \times 10^{13}$, and $[H_2S] = 2.3 \times 10^{13}$ molecules cm^{-3}; (b) with DMS, $[NO_2] = 1 \times 10^{14}$, $[OH] = 2 \times 10^{13}$, and $[DMS] = 6.4 \times 10^{13}$ molecules cm^{-3}; (c) with CH_3SH, $[NO_2] = 7.4 \times 10^{13}$, $[OH] = 2.0 \times 10^{13}$, and $[CH_3SH] = 5.6 \times 10^{13}$ molecules cm^{-3}. The experimental spectra have been corrected for response of the detector. The calculated spectra are shown by the dotted curves.

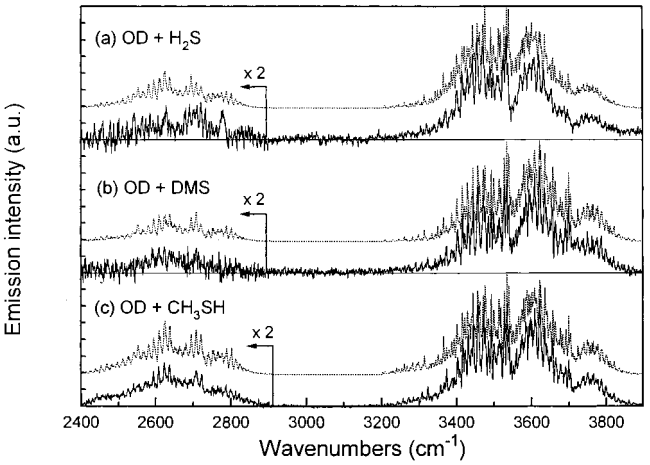

Figure 4. Infrared chemiluminescent spectra produced by the reactions of OD at 0.5 Torr ($\Delta t = 0.25$ ms): (a) with H_2S, $[NO_2] = 4 \times 10^{13}$, $[OD] = 1.6 \times 10^{13}$, and $[H_2S] = 1.3 \times 10^{13}$ molecules cm^{-3}; (b) with DMS, $[NO_2] = 1 \times 10^{14}$, $[OD] = 2.3 \times 10^{13}$, and $[DMS] = 4.0 \times 10^{13}$ molecules cm^{-3}; (c) with CH_3SH, $[NO_2] = 1 \times 10^{14}$, $[OD] = 2.3 \times 10^{13}$, and $[CH_3SH] = 2.3 \times 10^{13}$ molecules cm^{-3}. The experimental spectra have been corrected for the response of the detector. The calculated spectra are presented by dotted curves.

The HOD surprisal plots for model I in Figure 5a, which are plots of $-\ln(P_3/P°_3)$ vs f_{υ_3} ($=E_{\upsilon_3}/\langle E_{av}\rangle$), directly reflect the deviation of the excitation in the newly formed H−OD bond from the statistical expectation. The surprisal plot for OD + H_2S is linear with a slope of $-\lambda_{\upsilon_3} = 6.2 \pm 0.5$. A straight line drawn through the three points corresponding to $\upsilon_3 = 1$, 2, and

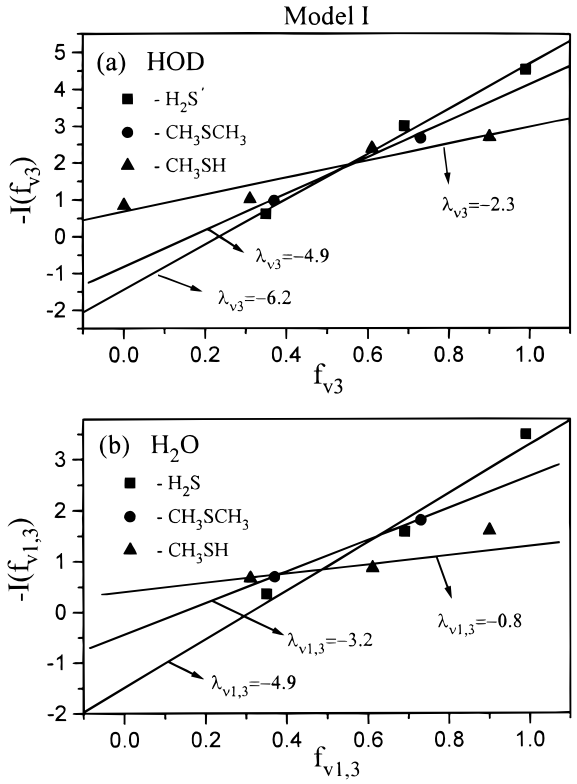

Figure 5. Surprisal plots for vibrational stretching distributions using model I for the prior: (a) HOD from the OD + H_2S, CH_3SCH_3 and CH_3SH reactions; (b) H_2O from the OH + H_2S, CH_3SCH_3, and CH_3SH reactions.

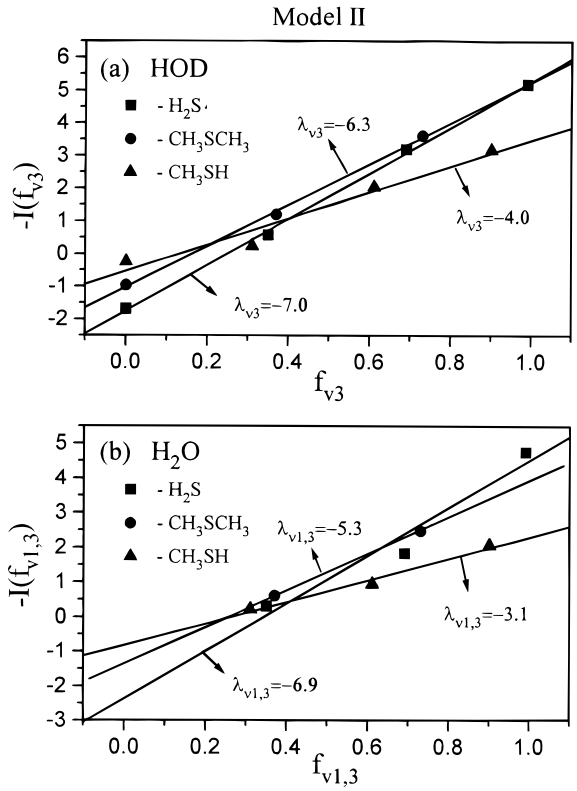

Figure 6. Surprisal plots for vibrational stretching distributions using model II for the prior: (a) HOD from the OD + H_2S, CH_3SCH_3, and CH_3SH reactions; (b) H_2O from the OH + H_2S, CH_3SCH_3, and CH_3SH reactions.

3, with neglect of $P_3(0)$ has an intercept of $\lambda^\circ_3 = -1.5 \pm 0.3$, giving $P_3(0) = 18 \pm 4$ and a renormalized total population $P_{1,3}(0{:}1{:}2{:}3) = (15 \pm 3){:}32{:}50{:}3$, in reasonable agreement with the measured value for $P_3(0) \approx 20$. The H_2O surprisal plot, $-\ln(P_{1,3}/P^\circ_{1,3})$ vs $f_{v_{1,3}}$ ($=E_{v_{1,3}}/\langle E_{av}\rangle$) presented in Figure 5b, has a smaller slope, since it is related to a mixture of the "active" and "spectator" local O−H mode vibrations, which are observed as a mixture of ν_1 and ν_3 normal modes. The distribution from reaction 1 has a linear surprisal with $-\lambda_{v_{1,3}} = 4.9 \pm 0.8$ and an intercept $\lambda^\circ_{1,3} = -1.4 \pm 0.5$, giving $P_{1,3}(0) = 14 \pm 4$, and the renormalized total distribution $P_{1,3}(0{:}1{:}2{:}3) = (12 \pm 3){:}44{:}41{:}4$. As expected, the slopes of the surprisal plots calculated using model II are steeper than for the model I and are equal to $-\lambda_{v_3} = 7.0 \pm 0.2$ and $-\lambda_{v_{1,3}} = 6.8 \pm 1.5$ (Figure 6). These intercepts would give smaller $P_{1,3}(0)$ and $P_3(0)$ values. Since the predictions of model I surprisals match the $P_3(0)$ value for H_2S obtained from the HOD measurements (with estimated populations in the dark states), we used model I surprisals to obtain $P_{1,3}(0)$ for H_2O. The bending distribution in $v_{1,3} = 0$ was estimated assuming a similarity with $v_{1,3} = 1$ and a geometric progression that decreased by a factor of 2 for the (050) and (060) states.

The distributions based on assignment of $P_3(0)$ and $P_{1,3}(0)$ from linear surprisal plots are thought to be the most reliable, and they were used to calculate the global averages. The total vibrational distribution gives the fraction of the available energy released as vibrational energy of H_2O as $\langle f_v\rangle = 0.58$ with the fraction in bending $\langle E_{2v}\rangle/\langle E_v\rangle = 0.24$. For reaction (1D), $\langle f_v\rangle = 0.61$, and the fraction released to the OH mode is $\langle E_{3v}\rangle/\langle E_v\rangle = 0.74$. The uncertainty in these global average fractions was estimated from the uncertainties in the simulation procedure to be ±0.02; the error limits in Table 4 also include the uncertainty in $\langle E_{av}\rangle$.

The OH and OD reactions with H_2S both exhibited a chemiluminescence in the 1800−1900 cm^{-1} range (Figure 7a). This emission has a clear P, Q, R structure with the Q-peak position at 1875 ± 2 cm^{-1}. The P- and R-branch lines are separated by approximately 3.5 cm^{-1}. This identifies the observed emission as the $^2\Pi$ ($v = 1 \rightarrow v = 0$) band of NO ($2B_e = 3.7$ cm^{-1}). The NO emission must be produced by reaction 4,

$$HS + NO_2 \rightarrow HSO + NO \qquad (4)$$

which has a rate constant of $k_4 = 5.8 \times 10^{-11}$ molecule^{-1} s^{-1}.[24] Reaction 4 probably competes with reaction 5,

$$HS + OH \rightarrow H_2O^{sec} + S \qquad (5a)$$

$$\rightarrow SO + H_2 \qquad (5b)$$

which could proceed by recombination with release of ~70 kcal mol^{-1} and subsequent decomposition via (5a) and (5b). The excitation energy was estimated from $\Delta H^\circ_f(HSOH)$[22] = −35.4 kcal mol^{-1}. Both channels are exothermic, $\Delta H^\circ_0 = -35.4$ kcal mol^{-1} for (5a) and $\Delta H^\circ_0 = -44.0$ kcal mol^{-1} for (5b). Numerical calculations for our typical conditions with [OH] = 2.3×10^{13} molecules cm^{-3} show that even for the largest possible rate constant for the secondary reaction 5a, $k_{5a} \approx 10^{-10}$ cm^3 molecule^{-1} s^{-1}, and a reaction time of $\Delta t = 0.25$ ms, the $[H_2O^{sec}]/[H_2O]$ ratio does not exceed 0.08, and channel 5a does not affect the water spectrum from reaction 1. The SH + NO reaction is very slow[24] and can be neglected.

TABLE 4: Summary of Energy Disposal for OH, OD and F + RSR′ Reactions and Reactions of OD with HBr, HI and Hydrocarbons

reaction	$\langle E_{av}\rangle$[a]	$-\lambda_{vn}$[b] I	$-\lambda_{vn}$[b] II	$\langle f_v\rangle$	$\langle E_{vs}\rangle/\langle E_v\rangle$[c]	ref
$OH + H_2S \rightarrow H_2O + HS$	32.1	4.9	6.9	0.58	0.24	
$OH + DMS \rightarrow H_2O + CH_3SCH_2$	27.5	3.2	5.3	0.53	0.30	
$OH + CH_3SH \rightarrow H_2O + CH_3S$	34.4	0.8	3.1	0.38	0.41	
$OD + H_2S \rightarrow HDO + HS$	32.4	6.2	7.0	0.61	0.74	
$OD + DMS \rightarrow HDO + CH_3SCH_2$	27.8	4.9	6.3	0.55	0.64	
$OD + CH_3SH \rightarrow HDO + CH_3S$	34.7	2.3	4.0	0.43	0.36	
$OH + HBr \rightarrow H_2O + Br$	33.7	4.5		0.61	0.30	2
$OD + HBr \rightarrow HDO + Br$	34.0	6.1		0.63	0.61	2
$OH + C_6H_{12} \rightarrow H_2O + C_6H_{11}$	27.1	5.7	8.2	0.62	0.14	3
$OH + C_4H_{10} \rightarrow H_2O + C_4H_9$	24.7	5.5	8.4	0.65	0.19	3
$OD + C_6H_{12} \rightarrow HDO + C_6H_{11}$	27.4	6.3	8.6	0.56	0.82	3
$OD + C_4H_{10} \rightarrow HDO + C_4H_9$	25.0	6.3	8.6	0.59	0.79	3
$F + H_2S \rightarrow HF + HS$	47.8	3.2	7.0	0.45		31
$F + DMS \rightarrow HF + CH_3SCH_2$	44.8	4.1	6.2[d]	0.45[e]		32
				0.40−0.49		33

[a] In kcal mol^{-1}. Available energies for deutero-isotopic reactions were calculated accounting for a change in zero vibration energies. [b] Model I neglects internal degrees of freedom of the product radical in the calculation of prior distribution; model II includes rotations of the radical fragment. [c] The fraction of the total vibrational H_2O energy released to bending mode, $\langle E_{v_2}\rangle/\langle E_v\rangle$, in reactions with OH and the fraction of HOD vibrational energy found in O−H mode, $\langle E_{v_3}\rangle/\langle E_v\rangle$, for reactions with OD. [d] By analogy to $F + CH_3OCH_3$ from ref 34. [e] Population in $v = 0$ is neglected.

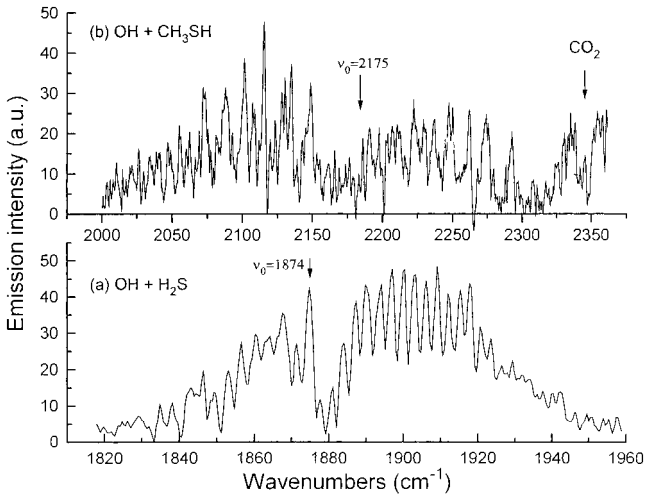

Figure 7. Infrared chemiluminescence in the long wavelength region observed from the reactions of OH with H_2S (a) and CH_3SH (b). (a) Same reaction conditions as for Figure 1a. The spectrum is assigned to the $1 \rightarrow 0$ fundamental band of NO($^2\Pi$). (b) Same reaction conditions as for Figure 1c. This spectrum has not been assigned.

3.2. Reactions of OH and OD with CH_3SCH_3. The H_2O and HOD spectra from reactions 2 and 2D are shown in Figures 3b and 4b, respectively, for the reactant concentrations indicated in the figure captions. The best-fit simulated spectra correspond to the distributions given in Tables 2 and 3. The $P_{1,3}(v_{1,3}) =$ 67:34 distribution of H_2O shows a decreasing population for the stretching levels. The bending distribution of the $v_{1,3} = 1$ level has a slight inversion with a maximum population in $v_2 = 1$. The $P_3(0{:}1{:}2) = 25{:}48{:}27$ distribution of HOD has a clear maximum for $v_3 = 1$.

The surprisal plot for HOD (circles in Figure 5a) is linear with a slope of $-\lambda_{v_3} = 4.9 \pm 0.3$. A straight line drawn through the two better defined points corresponding to $v_3 = 1$ and $v_3 = 2$ has an intercept of $\lambda^\circ_3 = -0.88 \pm 0.23$, giving $P_3(0) = 34 \pm 4$ and the renormalized total population $P_3(0{:}1{:}2{:}3) = (33 \pm 4){:}43{:}24$, in reasonable agreement with the $P_3(0) = 25$ obtained from fitting the 2400−2800 cm^{-1} band in the spectrum. As for the reaction with H_2S, the H_2O, surprisal plot (Figure 5b) shows a smaller slope than that for HOD, $-\lambda_{v_{1,3}} = 3.2$. The intercept of the linear fit for $v_3 = 1$ points is $\lambda^\circ_{1,3} = -0.45 \pm 0.12$, giving $P_{1,3}(0) = 39 \pm 5$, and the renormalized total population is $P_{1,3}(0{:}1{:}2) = (28 \pm 4){:}48{:}24$. The uncertainties in λ°_3 and $\lambda^\circ_{1,3}$ were determined from the limiting populations ratio $P_{1,3}(1)/P_{1,3}(2) = 1.99 \pm 0.18$ for H_2O and $P_3(1)/P_3(2) = 1.78 \pm 0.12$ for HOD, corresponding to the standard deviations of the populations. The surprisal plots calculated using model II prior shown in Figure 6 are linear with the slopes $-\lambda_{v_3} = 6.3$ and $-\lambda_{v_{1,3}} = 5.3$. The global averages were calculated from the distributions that used $P_{1,3}(0)$ and $P_3(0)$ values from extrapolation of model I surprisals. The fractions of the available energy released as vibrational energy are $\langle f_v(H_2O)\rangle = 0.52 \pm 0.02$ and $\langle f_v(HOD)\rangle. = 0.53 \pm 0.02$. The overall uncertainty given in Table 4 is 2 times larger because of the uncertainty of the thermochemistry. From the P_2 distribution of H_2O and from the P_3 distribution of HOD, the fraction of the vibrational energy released to bending is $\langle E_{2v}\rangle/\langle E_v\rangle = 0.30$, and the fraction disposed to O−H stretching is $\langle E_{3v}\rangle/\langle E_v\rangle = 0.64$.

The most probable secondary reactions of the CH_3SCH_2 radical for our experimental conditions are given below:

$$CH_3SCH_2 + NO_2 \rightarrow CH_3SCH_2O + NO \quad (7)$$

$$CH_3SCH_2 + NO + M \rightarrow CH_3S(NO)CH_2 + M \quad (8)$$

$$CH_3SCH_2 + OH \rightarrow CH_3SCH_2OH \rightarrow \text{products} \quad (9)$$

However, no emissions, except from H_2O and HOD, were observed from the DMS reaction system.

3.3. Reactions of OH and OD with CH_3SH. The H_2O and HOD spectra from reactions 3 and 3D are shown in Figures 1d and 2d, respectively, as well as in Figures 3 and 4. The best-fit simulation spectra are presented by dotted curves in Figures 3 and 4 for the vibrational distributions given in Tables 2 and 3. The H_2O stretching distribution is $P_{1,3}(1{:}2{:}3) = 69{:}28{:}3$. The bending distribution of the $v_{1,3} = 1$ level has a slight inversion with maximum population in $v_2 = 1$. In strong contrast to reactions 1D and 2D, the P_3 distribution of HOD decreases monotonically with v_3, and the best fit was $P_3(0{:}1{:}2{:}3) = 63{:}22{:}15{:}1$. The larger $P_3(0)$ population is clearly evident from the stronger emission in the 2400−3000 cm^{-1} range of Figure 4, and $P_3(0)$ could be rather accurately determined by simulation of the experimental spectrum for reaction 3D. Although they are small, the populations in $v_{1,3} = 3$ and $v_3 = 3$ levels and the

more extensive $P_2(v_2)$ populations, relative to reaction 2, signify that channel 3a must be important to some extent.

The surprisal plots with a model I prior are shown in Figure 5 for $\langle E_{av}\rangle = 34.4$ (or 34.7). The slope of the linear surprisal plot for P_3 of HOD (triangles in Figure 5a) is $-\lambda_{v_3} = 2.3 \pm 0.5$. The intercept is $\lambda^\circ_3 = 0.70 \pm 0.15$, giving $P_3(0) = 153 \pm 22$ and a renormalized total population $P_3(0{:}1{:}2{:}3) = (60 \pm 4){:}24{:}15{:}1$. The H_2O stretching vibrational surprisal plot (Figure 5b) shows less decline than that for HOD, $-\lambda_{v_{1,3}} = 0.78 \pm 0.04$. The intercept is $\lambda^\circ_{1,3} = 0.44 \pm 0.12$, giving $P_{1,3}(0) = 79 \pm 7$ and the renormalized total population $P_{1,3}(0{:}1{:}2{:}3) = (45 \pm 3){:}39{:}16{:}1$. Surprisal plots calculated using model II prior shown in Figure 6 give $-\lambda_{v_3} = 4.0 \pm 0.6$ and $-\lambda_{v_{1,3}} = 3.1 \pm 0.4$. Their intercepts would give somewhat lower estimates for $P_3(0)$ and $P_{1,3}(0)$. The assignments of $P_3(0)$ and $P_{1,3}(0)$ are very important because our choices dictate a different type of vibrational distribution for reaction 3 vs reactions 1 and 2. The experimental spectra in the 2400−3000 cm^{-1} region for (3D), as well as the surprisal extrapolations, are consistent with the distributions summarized in Tables 2 and 3. The calculated fraction of the energy released to H_2O was found to be $\langle f_v(H_2O)\rangle = 0.39 \pm 0.01$ and with the fraction disposed to bending, $\langle E_{2v}\rangle/\langle E_v\rangle, = 0.41$. The $\langle f_v(HOD)\rangle$ is 0.36 ± 0.01, with the fraction released to the OH stretch, $\langle E_{3v}\rangle/\langle E_v\rangle, = 0.44$. The uncertainty in the available energy increases the overall uncertainty of the energy disposal fractions to ±0.02. The sum of $\langle E_{2v}\rangle/\langle E_{av}\rangle$ and $\langle E_{3v}\rangle/\langle E_{av}\rangle$ is just 0.85, suggesting that some energy actually is released directly to the old bond of water in reaction 3.

The integrated emission intensities from H_2O and HOD molecules can be compared for the DMS and CH_3SH reactions. The H_2O emission intensity ratio from reactions 2 and 3 for equal reactant concentrations was $I_2/I_3 = 0.18$, with an accuracy of about 5%. Adjustment for the vibrational distributions transforms this value to a concentration ratio of 0.15 in favor of reaction 3. Analogous data for reactions 2D and 3D give $I_{2D}/I_{3D} = 0.14$ and a HOD concentration ratio of 0.12. These concentration ratios actually are very close to the rate constant ratio of Table 1, and our data show that reaction 3 occurs mainly by formation of water. Taking the experimental value of the secondary kinetic-isotope effect for the DMS reaction, $k_{OH}/k_{OD} = 0.85 \pm 0.07$ reported by Stickel et al.,[9] we obtain an even larger inverse secondary kinetic isotope effect for the CH_3SH reaction of $k_{OH}/k_{OD} = 0.85-(0.12/0.15) = 0.68$. The expected small inverse isotope effect for reactions of OD radicals was discussed in ref 3.

In addition to water emission, a distinct emission in the 2000−2300 cm^{-1} range was observed from the reactions with CH_3SH (Figure 7b). This spectrum has an apparent P and R structure with a band center of $\nu_0 \approx 2175 \pm 20$ cm^{-1}. The approximate intervals between the peaks in the rotational structure of the band are 15 cm^{-1}. A possible candidate for this emission is the HSO radical with $\nu_1 = 2271$ cm^{-1} (H−S stretch), $\nu_2 \approx 1100$ cm^{-1} (bend), and $\nu_3 \approx 1020$ cm^{-1} (S−O stretch).[30a] Another measurement[30b] gave $\nu_1 = 2570$ cm^{-1}, but both values are indirect estimates from spectra of the electronic $^2A'-^2A''$ transition of HSO. The HSO radical is nearly a symmetric prolate top with rotational constants $A_e \approx 9$ cm^{-1}, $B_e \approx 0.70$, and $C_e \approx 0.65$ cm^{-1}, as calculated from its equilibrium geometry R(H−S) = 1.37 Å, R(S−O) = 1.49 Å, and ∠(H−S−O) = 106°.[21] The observed peaks could represent two sets of Q-branch heads for $\Delta\nu_1 = -1$ transitions from $v_1 = 1$ and $v_1 = 2$ states. The possible secondary reactions involving CH_3S in our reactor are as follows:

$$CH_3S + NO_2 \rightarrow CH_3SO + NO \quad (10)$$

$$CH_3S + NO + M \rightarrow CH_3S(NO) + M \quad (11)$$

$$CH_3S + OH \rightarrow CH_3SOH \rightarrow CH_4 + SO \quad (12a)$$

$$\rightarrow H_2O + CH_2S \quad (12b)$$

$$\rightarrow CH_3 + SOH \quad (12c)$$

The rate constants are $k_{10} = 5.6 \times 10^{-11}$ and $k_{11} = 3.2 \times 10^{-29}$ [M] $\approx 10^{-12}$ cm^3 $molecule^{-1}$ s^{-1},[23] and reaction 11 can be neglected. Reaction 12 has not been studied, and we suppose that it proceeds via association of CH_3S and OH followed by decomposition with elimination of CH_4 (12a) or H_2O (12b) or cleavage of the C−S bond (12c). Energetically, channel 12a is the most preferable, $\Delta H^\circ = -55.5$ kcal mol^{-1}, compared to $\Delta H^\circ \approx -30$ kcal mol^{-1} for channel 12b and $\Delta H^\circ = -9.2$ kcal mol^{-1} for channel 12c. The SOH isomer is 5.4 kcal mol^{-1} less stable than HSO, but the barrier for isomerization was calculated to be of the order of 40 kcal mol^{-1},[21] so that formation of the HSO isomer in reaction 12 is rather probable. The source of the observed emission in Figure 7b remains an unanswered question.

4. Discussion

The section is organized so as to proceed from a discussion of mechanisms to items of a more dynamical nature. An important general experimental observation from this work is that H_2O(HOD) formation comprises the major part of the total rate constants given in Table 1. A summary of the energy disposal for reactions 1−3 and a few other reference reactions is presented in Table 4. The uncertainty quoted for CH_3SH is primarily from the simulation procedure. The greater uncertainty in the thermochemistry and E_a values is responsible for the larger uncertainties quoted in Table 4 for the $\langle f_v\rangle$ of H_2S and $(CH_3)_2S$. The assignments of $P_3(0)$ and $P_{1,3}(0)$ based on model I as the prior were used to calculate the global averages of Table 4 because the experimentally measured $P_3(0)$ values of HOD agree better with the result from surprisal plots using a model I prior. The surprisal plots for a model II prior are still linear, but the $-\lambda_v$ values are larger (see Table 4) and the intercepts give a somewhat smaller $P_3(0)$ or $P_{1,3}(0)$ contribution. The observation of v_3 and $v_{1,3} = 3$ from the CH_3SH reaction identified channel 3a from the energy balance. We used $\langle E_{av}\rangle$ from reaction 3 (3D) as 34.4 (34.7) kcal mol^{-1}, assuming that (3a) is the only product channel in computing the entries in Table 4. The lower population of v_3 and $v_{1,3} = 2$, relative to the H_2S reaction, could arise via a contribution from 3b competing with (3a) or it could be just (3a), but with a mechanism differing from that of H_2S. The 4-fold larger $P_3(0)$ observed from the $\Delta v_{1,2} = -1$ spectra supports the latter. On the basis of the product vibrational distribution, we argue below that the dominant mechanism for OH + CH_3SH is attack at the sulfur atom followed by rearrangement to give H_2O from the S−H side of the adduct. Presumably "direct" abstraction also occurs with rate constants (per C−H or S−H bond) similar to those for (1) and (2), but these contributions to the total H_2O yield will be minor.

Comparison of the vibrational distributions and the $\langle f_v\rangle$ vales of H_2O and HDO from reactions 1−3 and 1D−3D identifies a difference between the "symmetric" molecules H_2S and DMS vs CH_3SH. Reactions 1D and 2D give inverted O−H stretching distributions in HOD peaking on $v_3 = 2$ (H_2S) and $v_3 = 1$

(DMS), whereas a decreasing P_3 distribution was obtained from the CH_3SH reaction. The bending distributions in H_2O from all three OH reactions are generally close to the statistical limit for model I prior, with some underpopulation of $v_2 = 0$ and overpopulation of $v_2 = 1$ levels; however, the large $P_{13}(0)$ and $P_3(0)$ population with higher bending energy raises the fraction of bending energy for reaction 3. The similar values of $P_{1,3}(0)$ and $P_3(0)$ for the H_2S and DMS reactions show that the old O−H (O−D) bond of hydroxyl is not strongly involved in the reaction dynamics. This conclusion also is supported by the similarity of the $P_{1,2}$ and P_2 distributions, although the more extended range of populated $v_{1,2}$ levels for HOD suggests that some v_1 excitation actually does occur. These $P_{1,2}$ distributions of HOD appear to be "cooler" than the prior distributions $P^\circ_{1,2}$ (even for model II prior, not shown here). Thus, the excitation in the ν_1 mode is less than statistical, since the bending distribution is nearly statistical, as shown by comparing the P°_2 and P_2 distribution of H_2O in Table 2. A spectator nature for the "old" OH bond seems approximately true for reactions 1 and 2, but not for reaction 3. This is shown most clearly in that $\langle E_{2v}\rangle/\langle E_v\rangle + \langle E_{3v}\rangle/\langle E_v\rangle$ only sums to 0.85. More difference also exists between $P_3(0)$ and $P_{1,3}(0)$ for reaction 3.

The available energies for the H_2S (32.1 kcal mol^{-1}) and HBr (33.7 kcal mol^{-1}) reactions are nearly the same and the temperature dependencies also may be similar, although the H_2S reaction has not been so extensively studied. Since HBr is thought to be representative for direct abstraction dynamics,[24] a detailed comparison is worthwhile. In fact, the H_2O and HOD distribution are nearly identical for both reactions. The P_3-(HOD) and $P_{1,3}(H_2O)$ surprisals are linear with $-\lambda_v(P_3) = 6.2$ vs 6.1 and $-\lambda_v(P_{1,3}) = 4.9$ vs 4.5 for the H_2S and HBr reactions, respectively. The $\langle f_v(H_2O)\rangle$ values are 0.58 vs 0.61, and the $\langle f_v(HOD)\rangle$ values are 0.61 vs 0.63. Detailed inspection of the distributions show very little difference, except for slightly more extended P_2 and $P_{1,2}$ distributions for HBr, which is evident by a lower ratio of stretch-to-bend excitation for HBr (2.0 vs 3.1). The mechanism for OH + H_2S certainly seems to be direct abstraction. The ab initio calculations[22] also favored direct abstraction, rather than adduct formation followed by rearrangement. In contrast to the OH reactions, the energy disposal from F atom reactions with H_2S and HBr is distinguishably different with $\langle f_v(HF)\rangle = 0.45$ vs 0.60, respectively, and with the vibrational distribution from HBr being much more inverted.[34]

The rate constants, per reactive C−H bond, for the $(CH_3)_2S$ and n-C_4H_{10} reactions are nearly the same, and comparison provides an opportunity to search for any difference from direct abstraction from C−H bonds, with recognition that $\langle E_{av}\rangle$ for $(CH_3)_2S$ is 2.8 kcal mol^{-1} larger than for n-C_4H_{10}. As shown in Table 4, the $\langle f_v(H_2O)\rangle$ and $\langle f_v(HOD)\rangle$ values from $(CH_3)_2S$ are nearly the same (∼0.54) and both are lower than those for C_4H_{10} (0.62 and 0.56). The $P_3(H_2O)$ and $P_{1,3}(HOD)$ distributions are more inverted for C_4H_{10}, as shown by its larger $-\lambda_v$ value, and the fraction of the vibrational energy released as stretching excitation is 2 times higher for C_4H_{10} than for DMS. The comparison of DMS with cyclohexane is similar, and in this case the $\langle E_{av}\rangle$ are the same. The mechanism for DMS seems to be direct abstraction from a C−H bond,[3] but the stretching distribution is less inverted and the bending mode gains energy at the expense of the stretch mode for H_2O (HOD) formation from DMS relative to the hydrocarbons. This is another example illustrating the sensitivity of the stretch-to-bend excitation ratio to the reactant for water-forming reactions.[1−3]

Just as for the H_2S reactions, the vibrational energy disposal[33] to HF(v) from F + $(CH_3)_2S$ is lower than for OH + $(CH_3)_2S$; $\langle f_v(H_2O)\rangle = 0.57$ vs $\langle f_v(HF)\rangle = 0.45$, and the linear surprisals have smaller slopes $-\lambda_{HOD} = 4.9$ vs $-\lambda_{HF} = 4.1$. The energy disposal for F + $(CH_3)_2S$ and $(CH_3)_2O$ seems very similar and the latter has been extensively discussed.[35] The $(CH_3)_2O$ molecule is thought to be an example of an F atom reaction in which the radical stabilization energy is not available to the HF product. The dynamics for H_2O formation seem to permit a better coupling of the available energy to the H_2O product, perhaps the bending mode of H_2O plays some role. From the vibrational and the rotational distributions of HF produced in F + DMS reaction, the presence of two microscopic routes (direct abstraction and formation of an adduct followed by elimination) was proposed by Dehe and Heydtmann.[33] On the contrary, the H_2S and DMS reactions with hydroxyl show no evidence for more than one microscopic channel, which also may be a factor in the difference in energy disposal between the F and OH reactions.

The ab initio calculations[17] for OH + CH_3SH found that the adduct was 1.4 kcal mol^{-1} higher in energy than the reactants, and the authors favored a mechanism involving attack at the SH bond without an activation barrier. The same level of calculations as used for OH + CH_3SH underestimated the $(CH_3)_2S$- -OH binding by ∼4 kcal mol^{-1}, so a small binding energy for $CH_3(H)S$- -OH cannot be excluded. The $CH_3(H)S$- -OH interaction is not very attractive, but it is not repulsive either because the electronic energies of the adduct and transition state are nearly equal. The absence of a significant primary kinetic isotope effect[15,16] for OH + CH_3SD (CD_3SH) is additional experimental evidence in favor of a mechanism that does not involve breaking a S−H (or C−H) bond in the rate-determining step. The vibrational energy distributions from (3) and (3D) differ from those of reactions 1 and 2 in terms of $\langle f_v\rangle$, the ratio of the stretch-to-bend excitation, and the shape of the stretch distribution. All the experimental data point to a mechanism that is not mainly direct H atom abstraction. We suggest that the OH reacts by approaching the S atom, as well as the S−H end of the molecule, without a specific orientation; i.e., the entrance channel is not so narrow as that for direct abstraction,[34] and, hence, the rate constant is enhanced relative to reaction 1. Based upon the fact that the $(CH_3)_2S$−OH adduct cannot eliminate H_2O, but rather redissociates at room temperature, we favor elimination of water from the hydrogen end of the CH_3-SH·OH adduct to give mainly CH_3S.[6]

The observation of vibrationally excited NO from the OH + H_2S system suggests that reaction 4 proceeds through the formation of a HSONO complex, which subsequently decomposes by breaking the weakest bond. This motion corresponds to a reduction of the single-to-double bond S−O internuclear distances (R(S−O) = 1.69 Å in HSOH and 1.48 Å in HSO[16]) and shortening of the N−O distance (R(N−O) = 1.20 Å in NO_2 and R(N−O) = 1.15 Å in NO), and the NO could be excited. The enthalpy of (4) is $\Delta H^\circ_0 = -27.2$ kcal mol^{-1}, which could excite the stretching mode of both NO and HSO. Emission from the SO stretching mode of HSO ($\nu_3 \sim 1020$ cm^{-1})[16] is out of the range of the InSb detector. The weak emission observed in the 2000−3000 cm^{-1} range from the OH + CH_3-SH system could not be definitely assigned and requires further study.

5. Conclusions

The infrared emission from H_2O and HOD following the reactions of OH and OD radicals with H_2S, $(CH_3)_2S$, and CH_3-SH has been observed from a flow reactor. Comparisons of the total H_2O and HOD emission intensities from the $(CH_3)_2S$

and CH_3SH reactions confirm that water formation is mainly responsible for the larger rate constant of CH_3SH. The vibrational distributions of the H_2O and HOD molecules from OH and OD radicals reacting with H_2S, CH_3SCH_3, and CH_3SH were assigned by computer simulation of the spectra. All vibrational distributions extended to the thermochemical energy limit with an inverse correlation between stretching and bending excitation. The fraction of the available energy released as vibrational energy is $\langle f_v \rangle = 0.55$ for reactions with H_2S and $(CH_3)_2S$, but only $\langle f_v \rangle \cong 0.4$ for the reaction with CH_3SH. The H_2O and HOD stretching distributions from the H_2S and DMS reactions are inverted, whereas the stretching vibrational distribution from the CH_3SH reaction decreases with vibrational energy. The ratio of stretch-to-bend vibrational excitation was 2.7 and 2.1 for H_2S and $(CH_3)_2S$ and 1.1 for CH_3SH. Surprisal analysis of the distributions further illustrates different dynamics for reactions 1 and 2 vs reaction 3. Slopes of the linear surprisal plots were $-\lambda_{v_3} = 6.2$ and 4.9 for (1) and (2), while reaction 3 gave a substantially lower slope $-\lambda_{v_3} = 2.3$. These global measures of the energy disposal suggest that the H_2S and $(CH_3)_2S$ reactions proceed via direct hydrogen abstraction, while the CH_3SH reaction seems to proceed mainly by attack at the S atom followed by rearrangement giving water. The major rearrangement pathway involves the H from the hydrogen end of the molecule.[6,36] The energy disposal pattern from the H_2S and $(CH_3)_2S$ reactions resemble the results from other direct abstraction reactions.[1−3] In these cases, the old bond in the hydroxyl radical participates only marginally in the reaction dynamics (except to provide a bending coordinate), but it is not a pure spectator. One significant difference between abstraction from $(CH_3)_2S$ vs abstraction from typical secondary C−H bonds is the lower stretch-to-bend excitation ratio for $(CH_3)_2S$.

In addition to H_2O (or HOD) chemiluminescence, the NO($v = 1 \rightarrow v = 0$) emission was observed from the OH(OD) + H_2S system. Nitric oxide formation arises from the $HS + NO_2 \rightarrow HSO + NO$ secondary reaction.[5] The emission in the 2000−2400 cm^{-1} range observed in the OH(OD) + CH_3SH system, which also is from secondary reactions, needs further examination before the emitter can be identified.

Note Added in Proof. New experiments[36] of OH and OD + CH_3SD have confirmed[6] that abstraction of the deuterium atom is the predominant reaction pathway. Thus, the choice made for the thermochemistry for reactions 3 and 3D was correct.

Acknowledgment. The work done at Kansas State University was supported by the U.S. National Science Foundation, CHE-9505032.

References and Notes

(1) Butkovskaya, N. I.; Setser, D. W. *J. Phys. Chem*. **1996**, *100*, 4853.
(2) Butkovskaya, N. I.; Setser, D. W. *J. Chem. Phys*. **1997**, *106*, 5028.
(3) Butkovskaya, N. I.; Setser, D. W. *J. Chem. Phys*. **1998**, *106*, 2434.
(4) (a) Butkovskaya, N. I.; Muravyov A. A.; Setser, D. W. *Chem. Phys. Lett*. **1997**, *266*, 223. (b) Butkovskaya, N. I.; Setser, D. W. *J. Phys. Chem. A*, **1998**, to be published.
(5) Tyndall, G. S.; Ravishankara, A. R. *Int. J. Chem. Kinet*. **1991**, *23*, 483.
(6) Tyndall, G. S.; Ravishankara, *J. Phys. Chem*. **1989**, *93*, 4707.
(7) (a) Barone, S. B.; Turnipseed, A. A.; Ravishankara, A. R. *Faraday Discuss*. **1995**, *100*, 39. (b) Barone, S. B.; Turnipseed, A. A.; Ravishankara, A. R. *J. Phys. Chem*. **1996**, *100*, 14694.
(8) Turnipseed, A. A.; Barone, S. B.; Ravishankara, A. R. *J. Phys. Chem*. **1996**, *100*, 14703.
(9) (a) Stickel, R. E.; Zhao, Z.; Wine, P. H. *Chem. Phys. Lett*. **1993**, *212*, 312. (b) Hynes, A. J.; Wine, P. H.; Semmes, D. H. *J. Phys. Chem*. **1986**, *90*, 4148.
(10) Zhao, Z.; Stickel, R. E.; Wine, P. H. *Chem. Phys. Lett*. **1996**, *251*, 59.
(11) Hynes, A. J.; Stoker, R. B.; Pounds, A. J.; McKay, T.; Brandshaw, J. D.; Nicovich, J. M.; Wine, P. H. *J. Phys. Chem*. **1995**, *99*, 16967.
(12) Gu, M.; Turecek, F. *J. Am. Chem. Soc*. **1992**, *114*, 7146.
(13) McKee, M. L. *J. Phys. Chem*. **1993**, *97*, 10971.
(14) Hatakeyama, S.; Akimoto, H. *J. Phys. Chem*. **1983**, *87*, 2387.
(15) Hynes, A. J.; Wine, P. H. *J. Phys. Chem*. **1987**, *91*, 3672.
(16) Wine, P. H.; Thompson, R. J.; Semmes, D. H. *Int. J. Chem. Kinet*. **1984**, *16*, 1623.
(17) Wilson, C.; Hirst, D. M. *J. Chem. Soc., Faraday Trans*. **1995**, *91*, 3783.
(18) Leu, M.-T.; Smith, R. H. *J. Phys. Chem*. **1982**, *86*, 73.
(19) Michael, J. V.; Nava, D. F.; Brobst, W. D.; Borkowski, R. P.; Stief, L. J. *J. Phys. Chem*. **1982**, *86*, 82.
(20) Lin, Y.-L.; Wang, N.-S.; Lee, Y.-P. *Int. J. Chem. Kinet*. **1985**, *17*, 1201.
(21) Xantheas, S. S.; Dunning, T. H., Jr. *J. Phys. Chem*. **1993**, *97*, 6616.
(22) Wilson, C.; Hirst, D. M. *J. Chem. Soc., Faraday Trans*. **1994**, *90*, 3051.
(23) (a) Lafage, C.; Pauwels, J. F.; Carlier, M.; Devolder, P. *J. Chem. Soc., Faraday Trans. 2* **1983**, *83*, 731. (b) Westenberg, A. A.; de Haas, N. *J. Chem. Phys*. **1973**, *59*, 6685.
(24) Atkinson, R.; Baulch, D. L.; Cox, R. A.; Hampson, R. F., Jr.; Kerr, J. A.; Troe, J. *J. Phys. Chem. Ref. Data* **1992**, *21*, 1125.
(25) Berkowitz, J.; Ellison, G. B.; Gutman, D. *J. Phys. Chem*. **1994**, *98*, 2744.
(26) Morley, J. P.; Lambert, I. R.; Mordaunt, D. H.; Wilson, S. H. S.; Ashfold, M. N. R.; Dixon, R. N.; Western, C. M. *J. Chem. Soc., Faraday Trans*. **1993**, *89*, 3865.
(27) Jefferson, A.; Nicovich, J. M.; Wine, P. H. *J. Phys. Chem*. **1994**, *98*, 7128.
(28) Rothman, L. S.; Gamache, R. R.; Tipping, R. H.; Rinsland, C. P.; Smith, M. A. H.; Benner, D. C.; Devi, V. M.; Flaud, J.-M.; Camy-Peyret, C.; Perrin, A.; Goldman, A.; Massie, S. T.; Brown, L. R.; Toth, R. A. The HITRAN Molecular Database: Editions of 1991 and 1992. *J. Quant. Spectrosc. Radiat. Transfer* **1992**, *48*, 469.
(29) Bernstein, R. B.; Levin, R. D. Role of Energy in Reactive Molecular Scattering: An Information-Theoretic Approach; Bates, D. R., Ed.; *Advances in Atomic and Molecular Physics*; Academic Press: New York, 1975; Vol. 11, p 216.
(30) (a) Ohashi, N.; Kakimoto, M.; Saito, S.; Hirota, E. *J. Mol. Spectrosc*. **1980**, *84*, 204. (b) Schurath, U.; Weber, M.; Becker K. H. *J. Chem. Phys*. **1977**, *67*, 110.
(31) Agrawalla, B. S.; Setser, D. W. *J. Phys. Chem*. **1986**, *90*, 2450.
(32) Duewer, W. H.; Setser, D. W. *J. Chem. Phys*. **1973**, *58*, 2310.
(33) Dehe, K.; Heydtmann, H. *Chem. Phys. Lett*. **1996**, *262*, 683.
(34) Nizamov, B.; Setser, D. W.; Wang, H.; Peslherbe, G. H.; Hase, W. L. *J. Chem. Phys*. **1996**, *105*, 9887.
(35) Holmes, B. E.; Setser, D. W. In *Physical Chemistry of Fast Reactions*; Smith, I. W. M., Ed.; Plenum Press: New York, 1980; Vol. 2, p 83.
(36) Butkovskaya, N. I.; Setser, D. W. *Chem. Phys. Lett.*, to be published.